P514973.PDF [Page: 3 of 12]

DRES-SL-1999-085

ELSEVIER

Biosensors & Bioelectronics 14 (2000) 861–869

BIOSENSORS BIOELECTRONICS

www.elsevier.com/locate/bios

Red diode laser induced fluorescence detection with a confocal microscope on a microchip for capillary electrophoresis

Guifeng Jiang [a], Said Attiya [a], Gregor Ocvirk [a], William E. Lee [b], D. Jed Harrison [a,*]

[a] *Department of Chemistry, W3-13 Chemistry West, University of Alberta, Edmonton, AB, Canada T6G 2G2*
[b] *P O Box 4000, Defence Research Establishment Suffield, Medicine Hat, AB, Canada T1A 8K6*

Received 1 July 1999, received in revised form 30 August 1999, accepted 17 September 1999

Abstract

A highly sensitive laser induced fluorescence (LIF) detection system based on a 635 nm laser diode and cyanine-5 (Cy-5) dye, is described for use with a planar, microfluidic, capillary electrophoresis (CE) chip. The CE-chip is able to determine a protein biological threat agent simulant, ovalbumin (Ov), by performing an immunoassay separation of Cy-5 labeled anti-ovalbumin from its complex with Ov, in under 30 s. A confocal, epiluminescent detection system utilizing a photomultiplier tube gave optimum results with a 400 μm pinhole, an Omega 682DF22 emission filter, a 645DRLP02 dichroic mirror, a 634.54 ± 5 nm excitation filter, and a Power Technology ACMO8 635 nm laser operated at 11.2 mW. Using this detector, a microchip CE device with a separation efficiency of 42 000 plates and an etch depth of 20 μm, gave a concentration detection limit of 9 pM Cy-5. This limit corresponds to the determination of 4560 injected molecules and detection of 900 of these molecules, given a probe volume of 1 6 pl and a probing efficiency of 20%. © 2000 Elsevier Science S.A. All rights reserved.

Keywords: Microfluidics; Affinity capillary electrophoresis; Capillary zone electrophoresis; Immunoassay, Simulant, Ovalbumin

1. Introduction

Planar microfluidic devices utilizing electrokinetic pumping may provide a powerful tool for automating the fluid handling steps required in many biological assays (Manz et al., 1992; Harrison et al., 1993; Seiler et al., 1993; Fan and Harrison, 1994; Jacobson et al., 1994; Colyer et al., 1997; Effenhauser et al., 1997; Hadd et al., 1997). Such systems offer an alternative to biosensors for the detection of biological threat agents, or complement such sensors by transporting the sample and reagent to the detector (Manz et al., 1992; Harrison et al., 1993; Colyer et al., 1997; Effenhauser et al., 1997). We have developed microfluidic devices (Chiem and Harrison, 1997, 1998a,b) capable of performing immunoassays which can be applied to the determination of threat agents. In these devices, samples and immunoreagents are mixed within 30–60 μm wide flow channels, allowed to react homogeneously, and then electrophoretically separated in order to determine the sample concentration (Chiem and Harrison, 1998a). These devices provide a means to automate immunoassays in the field, performing an analysis within 1–5 min. Reagent consumption on the order of 0.1–10 nl per assay has been achieved, which is of critical importance for reduced maintenance of a field-based instrument.

To date, gas phase lasers were the most common excitation source for laser induced fluorescence (LIF) detection on microfluidic chips (Manz et al., 1992; Jacobson et al., 1994; Effenhauser et al., 1997; Chiem and Harrison, 1998a). Such lasers are bulky and can be fragile, which makes them ill-suited to field applications. Yet LIF is so sensitive that it is one of the most preferred detection methods on-chip. The red diode laser family represents a more compact, portable source for LIF on a chip, as has been made clear by the fact that diode lasers have been used previously in capillary electrophoresis (CE), (Imasaka, 1996). Ligler et al. have shown they can also be used with optical fiber immunosensors in the field (Shriver-Lake et al., 1995; Narang et al., 1997). Early studies showed the promise of these lasers for detection in CE, but detection limits were poor (Imasaka et al., 1991; McDonnell and Pawliszyn,

* Corresponding author

0956-5663/00/$ - see front matter © 2000 Elsevier Science S A. All rights reserved
PII: S0956-5663(99)00056-1

P514973.PDF [Page: 4 of 12]

102-01795/

1991; Wu et al., 1992; Jansson and Roeraade, 1993; Krattiger et al., 1994). However, the concentration detection limits have since improved to 50–100 pM with a red diode laser (Chen et al., 1993; Chen, 1995; Mank and Yeung, 1995) and ~3 pM in aqueous solutions using a gas phase Ar^+ ion pumped solid state Ti/sapphire laser (Flanagan et al., 1995).

In this report we examine the use of cyanine-5 (Cy-5) dye and Cy-5 labeled immunoreagents with a 635 nm diode laser and a microfluidic chip. The optimal parameters needed to obtain good detection limits with a confocal, epiluminescent microscope are reported. This microscope design was selected because it produced the best detection limits obtained on a chip when using a 488 nm LIF source (Ocvirk et al., 1998).

2. Experimental section

2.1. Devices

Microchannels were isotropically etched in 3 × 3" Pyrex glass (Paragon Optical, Reading, PA) and 4 × 4" 0211 glass (Corning, Corning, NY) as described previously (Fan and Harrison, 1994; Chiem and Harrison, 1998b). After drilling 1.9 mm diameter access holes in the cover plate, it was thermally bonded to the etched glass wafer to form an enclosed fluidic device. The chip layouts used in this study, COPI (Manz et al., 1992; Chiem and Harrison, 1997, 1998b) and DARPA1-NC, are depicted in Fig. 1. The device channels were etched either 13 or 20 μm deep, giving the channel width at the top indicated in Table 1. Pyrex COPI devices were used for all optical optimization procedures. Corning 0211 DARPA1-NC devices were used for measuring the limit of detection and the separation efficiency observed for a Cy-5 standard.

2.2. Materials

The unreactive Cy-5 standard dye was from Beckman Instruments (Fullerton, CA), (L +) lactic acid and boric acid were from Sigma (St. Louis, MO) and Baker (Phillipsburg, NJ), respectively. Water from a Milli-Q UV Plus Ultra-pure system (Millipore, Mississauga, ON, Canada) was used for all solutions. The borate buffer containing 0.2 mM (L +) lactic acid and 15 mM boric acid was adjusted to pH 10.6 with 1 M NaOH. A 10^{-7} M stock solution of Cy-5 dye was prepared by dissolving 200 picomoles of dye in 2 ml water. All

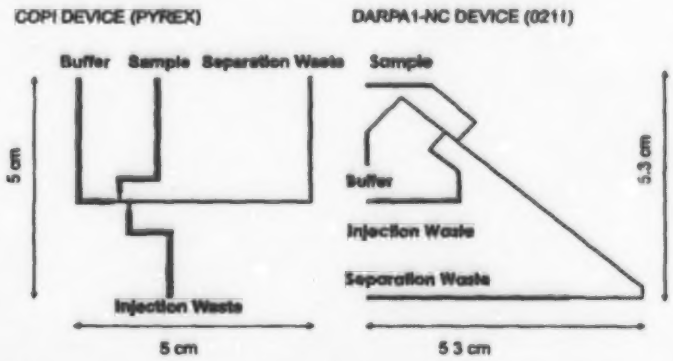

Fig. 1. Schematic layout of microchip design for COPI and DARPA1-NC devices. Reservoir junctions are indicated by their names. The double T injector offset is 100 μm in COPI, and 491 μm in DARPA1-NC device, they are exaggerated here for clarity. Channel widths are given in Table 1.

Table 1
Channel depths and widths[a]

Device	Depth (μm)	Feature width[b]		Etched width	
		Wide (μm)	Narrow (μm)	Wide (μm)	Narrow (μm)
COPI	13	210	25	260	78
COPI	20	210	25	284	96
DARPA1-NC	13	210	26	240	65
DARPA1-NC	20	210	26	270	75

[a] Channels are approximately trapezoidal in cross-sectional shape, with the etched width defining the upper width and the feature width defining the lower width. Dimensions were measured with a surface profilometer.

[b] Feature width defines the dimension on the photolithographic patterning mask.

P514973.PDF [Page: 5 of 12]

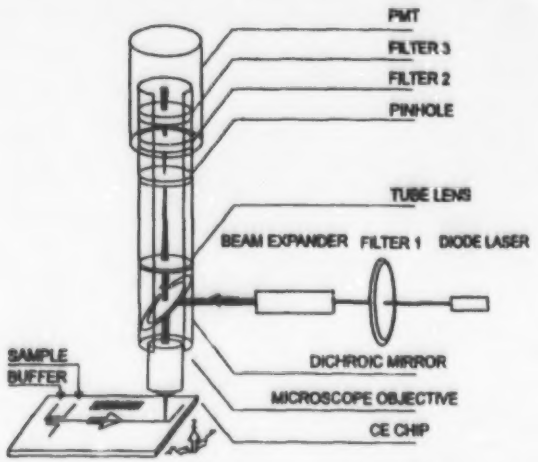

Fig. 2. Confocal epifluorescence setup for Cy-5 detection on chip

solutions used with Cy-5 were prepared by dilution of the stock solution in pH 10.6 borate buffers. Chicken egg ovalbumin and anti-ovalbumin were from Sigma. The antibody was labeled with bifunctional Cy-5 (Amersham Life Science, Pittsburgh, PA) using an affinity protected labeling procedure to be described elsewhere. A pH 8.5 buffer was prepared with 20 mM boric acid, NaOH added to adjust pH, and 20 mM NaCl. All chemicals used were reagent grade, and all solutions were filtered using 0.22 μm pore cellulose acetate syringe filters (Millipore, Bedford, MA) before use.

2.3. Instrumentation

A previously described (Seiler et al., 1993; Fan and Harrison, 1994; Chiem and Harrison, 1997) computer-controlled power supply system (−15 kV, MJ Series, Glassman High voltage, Whitehouse station, NJ) with high voltage relays (30 kV, Kilovac, Santa Barbara, CA) was used for voltage control. The optical set up is shown in Fig. 2, and is similar to that described previously for a 488 nm source (Ocvirk et al., 1998). The chip was mounted onto an $X-Y-Z$ translation stage (Newport 423, Irvine, CA). A power adjustable 635 nm diode laser (ACM08 (635-15) X 12, Power Technology Inc., Mabelvale, AR), was used as the exciting laser source. The laser light passed through an optional filter 1, a beam expander (optional, 10–20 × zoom, Edmund Scientific Company, NJ), then was reflected by a dichroic mirror (Omega, Battleboro, VT) and focused in the channel by a 0.6 NA, 40 ×, 4.9 mm focal length, 3.3 mm working distance microscope objective (Planachromat LDN 1 2-A, Carl Zeiss, Jena, Germany). The 670 nm (peak max) fluorescence signal, collected by the microscope objective, was passed through the dichroic mirror, then was focused by the tube lens (Achromat, Newport PAC064, $f=200$ mm) onto a pinhole located at the focal point and was detected by a photomultiplier tube (PMT, Hamamatsu R1477; bias: 900 V). Filter 2 and filter 3 (optional) were inserted above the pinhole for spectral filtering. Optical filters were purchased from Melles Griot (03F1L024, $\lambda_{max}=634.54$ nm, FWHM = 10 nm), Omega Optical (670DF40, 682DF22, 645DRLP02, 670DRLP02; Battleboro, VT) and Beckman (675DF20; Fullerton, CA). A 665 nm long pass filter was obtained from Rolyn Optics (RG665, Covina, CA). The laser power was measured using a Model 835 optical power meter (Newport). The PMT current was converted to a voltage using a 10^8 gain trans-impedance amplifier, filtered with an 8th order, active, 25 Hz, low-pass noise filter, then acquired with a Macintosh IIci computer. The National Instruments NB-MIO16 A/D board sampling rate was 50 Hz. All data was smoothed using a 21 point box smooth algorithm, included in Igor Pro (Wavemetrics, Lake Oswego, OR).

A Beckman P/ACE 5000 equipped with a 635 laser module LIF detector and a 27 cm long, 50 μm i.d. fused silica capillary operated at 20 kV, was used for comparative studies. The pressure injection mode was used for 10 s for sample introduction.

2.4. Chip operation

All devices were conditioned with 0.1 M NaOH for 30 min before use. The chip was then filled with Cy-5 solution after an intermediate rinsing step with borate buffer for 5 min. The dye or buffer solutions were flushed through the separation channel by applying vacuum at the separation waste port, resulting in a volume flow rate, u, of 3.8 μl/min. The flow rate was measured by determining the volume delivered over a 2 h period. The pinhole was positioned in the XY plane with a pinhole translator (Newport LP-1-XYZ) in order to obtain maximum fluorescence signals for a given dye concentration. The maximum background corrected fluorescence signal at a given Cy-5 concentration was found by monitoring the response for Cy-5 and buffer solutions ($u=3.8$ μl/min), while translating the chip vertically. The sectioning power study was done in continuous-flow mode. First, the chip was filled with buffer; the background data were collected while vertically scanning the chip from 40 μm below the focal plane to 40 μm above the plane in 1 μm steps. Then 10^{-8} M Cy-5 fluorescence signals were collected in the same way. The background corrected fluorescence signals in continuous flow experiments are the average of 3000 data points. The reported noise levels represent the standard deviation of the buffer background fluorescence ($n=3000$). Signal to noise ratios, S/N, were determined by dividing the background corrected fluorescence signal by the standard deviation.

P514973.PDF [Page: 6 of 12]

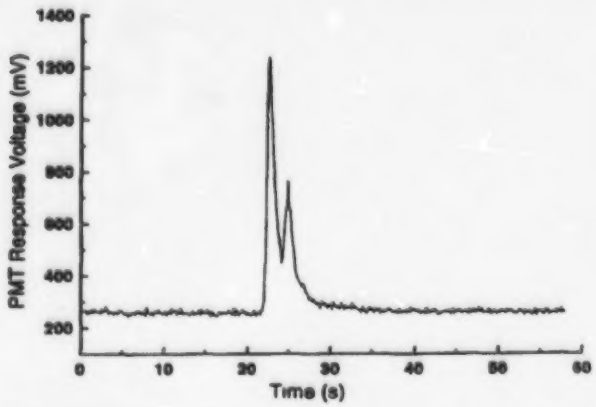

Fig 3 Electropherogram of a mixture of 200 nM Cy-5 labeled anti-ovalbumin, which appears first, and 600 nM ovalbumin, giving the antibody–antigen complex as a second peak, as obtained in DARPA1-NC.

For the evaluation of detection limits by capillary electrophoresis, the sample reservoir was filled with Cy-5 dye, and the others with buffer. A double T geometry was employed for injection, and an injection voltage of −2 kV was applied from sample to injection waste for an injection time of 10 s for all experiments. A separation voltage of −4 kV was subsequently applied from the buffer to the separation waste reservoirs. The S/N for each electropherogram was calculated by dividing the average peak height above background by the standard deviation in the background, determined from the portion of the electropherogram ($\Delta t = 20$ s) before the peak.

Solutions of antigen and Cy-5 labeled antibody were placed in the sample reservoir 5 min after mixing them together. An injection voltage of −1.2 kV was applied from sample to injection-waste reservoirs in DARPA1-NC for 3 s, after an initial 1 min flush. Separation was performed with −6 kV applied from the pH 8.5 borate buffer reservoir to separation waste.

3. Results and discussion

Separation of antibodies (Ab) from their antigen complexes using capillary electrophoresis can be a challenge, and the separation efficiency depends on the specific antigen/Ab pair (Grossman et al., 1989; Chu et al., 1994; Tao and Kennedy, 1996; Schmalzing and Nashabeh, 1997). The labeling dyes used often play a role, since they will change the charge to size ratio of the labeled compound. For this reason we evaluated our ability to separate Cy-5-labeled antibody to ovalbumin (Ab*) from the ovalbumin–Ab* complex. Ovalbumin (Ov) is a commonly used simulant for protein toxins in environmental trials. Figure 3 shows the separation of a mixture of 200 nM Ab* and 600 nM Ov, within a 13 μm deep DARPA1-NC device. The free Ab* eluted at 23 s, so the later eluting peak can be assigned to the antibody–antigen complex. The high concentration of Ov was needed because of the low affinity constant of this monoclonal antibody.

The results illustrate that the Cy-5/635 nm laser diode combination can be used for the LIF determination of immunoreaction products on a microfluidic chip. Optimization of the limits of detection (LOD) of this system was required for it to be used effectively. The relevant elements of our optimization study are discussed below. Key features included the choice of optical filter set, laser spot size, confocal pinhole choice and the volume of the detection channel.

3.1. Optimization of filters

Filter selection was difficult due to the small Stokes shift of the Cy-5 dye. Table 2 indicates the filter sets

Table 2
Evaluation of filter sets[a]

Filter 1	Dichroic mirror	Filter 2	Filter 3	Minimum detected Cy-5 concentration (nM)	LOD[b] (nM)
None	645DRLP02	670DF40	None	>10	
None	645DRLP02	682DF22	None	0.5	0.30[c]
None	645DRLP02	682DF22	665 long pass		0.20
634.54 ± 5 nm	645DRLP02	682DF22	None	0.1	0.15[c]
634.54 ± 5 nm	670DRLP02	682DF22	665 long pass	0.5	0.30
634.54 ± 5 nm	670DRLP02	675DF20	665 long pass		0.25
634.54 ± 5 nm	670DRLP02	670DF40	665 long pass	0.5	0.21
634.54 ± 5 nm	670DRLP02	670DF40	None	0.2	1.5[c,d]

[a] Refer to Fig. 2 for location of filters. This study was performed using a 200 μm diameter pinhole, 11.2 mW laser power (unexpanded beam) and a 13 μm deep COPI device.

[b] Limit of detection (LOD) extrapolated from replicate measurements ($n = 5$) at 1 nM Cy-5, except where marked (c).

[c] Extrapolated from plot of five different concentrations ranging from 0.5 to 10 nM.

[d] While the last filter combination entry, without the long pass filter, gave a measurable response at 0.2 nM, the sensitivity divided by the noise was ten times lower than for the best filter combination. This poor sensitivity accounts for the extrapolated LOD being much greater than 0.2 nM.

P514973.PDF [Page: 7 of 12]

examined. The specific locations of the filters are indicated in Fig. 2. The lowest detectable concentration we actually observed is given in Table 2, along with the LOD extrapolated from higher concentrations. The emission filter rejection power could be improved by adding a 665 nm long pass filter; however, we noted that the laser source could be viewed through the long pass filter alone. By instead using a laser line selection filter (634.54 ± 5 nm) between the laser and the excitation optics, the best LOD was obtained with a 645DRLP02 mirror and a 682DF22 filter. This result indicates the background emission of the laser at wavelengths considerably longer than 635 nm was significant compared to the dye's emission intensity, in agreement with Mank and Yeung (1995). This filter combination (row four of Table 2) provided the greatest value of sensitivity divided by noise of all the filter sets tested. With the exception of the data in Table 2, this filter set was used for all subsequent studies.

The data in Table 2 shows that use of the 670DRLP02 dichroic mirror, instead of the 645DRLP02 mirror, resulted in somewhat poorer LOD regardless of the other filter sets selected. Although the 670 mirror rejects more of the reflected 635 nm line than the 645 mirror, the improved transmission of the emitted light by the latter is apparently a more important factor, since the emission filters can be used to remove the laser line. The last two rows in Table 2 indicate that the 670DF40 emission filter was far too transmissive of the laser line, requiring the 665 nm long pass to provide satisfactory performance.

3.2. Optimization of excitation source

The effect of laser power and beam size is also significant, as a balance must be struck between the noise from elastic and inelastic scattering and the emission intensity, which will both increase with increasing power up to some limit (Mank and Yeung, 1995). Using an unexpanded laser beam, the optimized filter set and a 200 μm pinhole, the effect of laser power on the signal to noise ratio (S/N) was examined at 10 nM Cy-5. The S/N ratio increased linearly up to 6.2 mW of output power, and then remained essentially constant, up to the maximum of 13.0 mW. Plots of noise and of signal versus output power also followed the same trend. The results indicate that once the power exceeds a certain level the S/N performance saturates.

The output of a laser diode is astigmatic, with a different focal distance along the vertical and horizontal axes of the beam. This makes it difficult to focus the laser to a small, intense spot. The selected laser included prism-based optics to collimate the beam, and produce a near-Gaussian beam profile to allow better focusing. For a beam with a TEM 00 Gaussian profile the beam waist, w, is given by (Hecht and Zajac, 1974):

$$w = \lambda f/\pi w_o \quad (1)$$

where w_o is the incident beam radius, f is the focal length, and λ is wavelength, so long as w is above the diffraction limit of the lens. For the incident beam diameters used, Eq. (1) predicts spot sizes smaller than the diffraction limit. The diffraction limited spot diameter, d, can be determined from (Hecht and Zajac, 1974):

$$d = 1.22\ \lambda/\mathrm{NA} = 1.22\ \lambda/n\ \sin\ \alpha \quad (2)$$

where n is the index in which the lens is immersed, α is the angular semi-aperture, and NA is the numerical aperture. When the beam was expanded to give a collimated source 15 mm in diameter, a 10 μm spot was observed. The input diameter of the lens was 8.37 mm, so that it was totally filled by the expanded beam. Consequently, we used the stated NA of 0.6 to estimate a diffraction limited spot diameter of 1.3 μm. For the unexpanded laser beam the observed spot size was 18 μm in diameter, while a value of 1.9 μm is calculated from Eq. (2) using a value of α of 24.1, estimated from the geometry of the beam diameter and the focal length. The inability to focus to the diffraction limit must in large part be due to the astigmatic nature of the diode laser source, even with the correction optics. Note that the expanded beam is much better focused, even though the difference in the calculated diffraction limited spots for the two beams is rather small. When one considers that about 50% of the expanded beam radius is discarded by the lens aperture, it appears that the improved focus arises from eliminating non-Gaussian components from the beam profile.

Each optical component introduced losses in the laser power. The laser notch filter reduced the power to 54% of the initial value, while the dichroic mirror reduced the power to 90%, and the transmitted intensity through the lens was 38.5% of the incident power. For the expanded beam the expander reduced power to 55% of the incident intensity, while the 8.37 mm lens aperture resulted in a reduction to 50% of incident power. The latter is a greater reduction than the calculated drop to 74% for a 15 mm diameter beam, as estimated from the irradiance equation for a Gaussian beam (Hecht and Zajac, 1974). This result is again consistent with a notably non-Gaussian beam profile. Considering these loss factors and the observed spot sizes, the power density at the focal plane should be about 1000 W/cm^2 for the unexpanded beam, and 750 W/cm^2 for the expanded beam when using our typical incident laser power of 11.5 mW.

The depth of field, corresponding to a 5% expansion of the beam beyond the minimum beam waist, can be estimated from Eq. (3) (Hecht and Zajac, 1974):

$$\Delta z = \pm 0.32\pi w_o^2/\lambda \quad (3)$$

P514973.PDF [Page: 8 of 12]

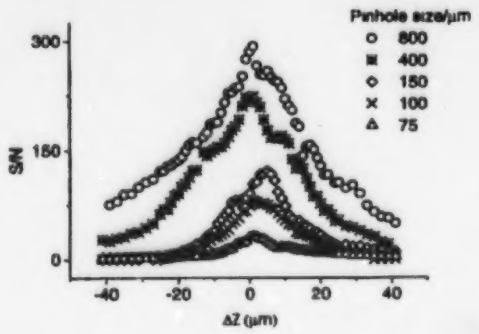

Fig 4 Signal-to-noise ratio versus vertical displacement of chip (Δz) for various pinhole diameters using a 13 μm deep channel, and an unexpanded laser beam A 10 nM Cy-5 standard solution was continuously flushed through the separation channel of a Pyrex COPI device by vacuum

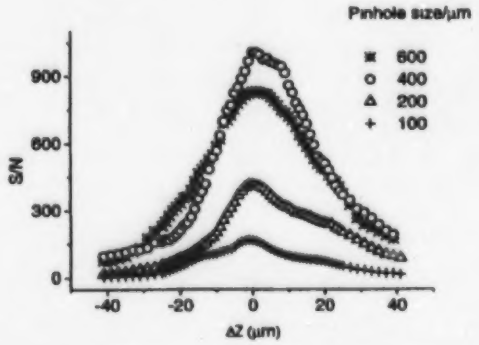

Fig. 5 Signal-to-noise ratio versus vertical displacement of chip (Δz) for various pinhole diameters using a 20 μm deep channel, and an expanded laser beam (see text) A 10 nM Cy-5 standard solution was continuously flushed through the separation channel of a Pyrex COPI device by vacuum

where w_o is the focused spot radius, and Δz is the vertical translation. From the observed 18 μm spot diameter we estimate a value of ±130 μm for the unexpanded beam. The depth of field estimated for the 10 μm spot created by the expanded beam is ±40 μm. Both spots are thus in focus over a much greater distance than the channel depth, so that scattering of the focused laser beam from the glass and the glass/solution interface will occur. Nevertheless, the expanded beam should produce less scatter, because it is focused over a much shorter distance. This was observed experimentally, as the beam expander reduced the noise from ±9.7 to ±4.0 mV when used with a 13 μm deep COPI device and a 200 μm pinhole.

3.3. Confocal sectioning power

The optical sectioning strength of a confocal microscope describes the manner in which fluorescence intensity changes with the axial distance between the objective lens and the object. Wilson (1989, 1990) defined the sectioning power as the full width at half maximum (FWHM) of intensity versus the axial displacement from the focal plane. In our present work we evaluated the sectioning power in 13 and 20 μm deep channels, filled with a continuous flow of 10 nM Cy-5 Background signal was measured with buffer moving in the flow channel at the same velocity. Figure 4 shows a plot of S/N versus axial displacement for a 13 μm deep, Pyrex, COPI device, using an unexpanded beam and several pinhole sizes. Significant distortion from a Gaussian profile is observed, which makes the FWHM values larger than those predicted by a linear extrapolation of Wilson's model (Wilson, 1989, 1990; Ocvirk et al., 1998) to the pinhole sizes we used. Figure 5 shows the results for a 20 μm deep, Pyrex, COPI device with which the beam expander was also used. The calculated and experimental results for both studies are presented in Table 3. The estimated theoretical sectioning power must be convoluted with a slit function model of the channel depth. The result is that the observed sectioning power should be equal to the calculated value when

Table 3
Observed and estimated confocal sectioning power

Pinhole diameter (μm)	Calculated sectioning power[a] FWHM (μm)	Observed sectioning power[b] FWHM (μm)	
		13 μm Deep	20 μm Deep
75	6 5	15 3	
100	8 2	18 4	31 6
150	11 7	19 5	
200	15 1		32 6
400	28 7	34 2	33 5
600	42 4		40 5
800	56 0	36 6	

[a] Estimated by linear extrapolation of Wilson's (1989, 1990) calculations The value does not include the affect of the slit function introduced by the channel depth (see text)
[b] Determined from Figs 4 and 5

P514973.PDF [Page: 9 of 12]

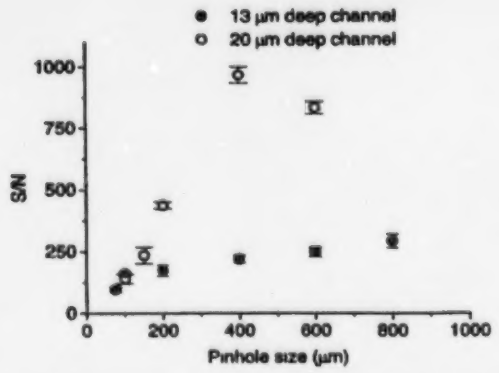

Fig. 6. Signal-to-noise ratio versus pinhole size for 13 and 20 μm deep channels in Pyrex COPI devices. A 10 nM Cy-5 standard solution was continuously flushed through the separation channel by vacuum.

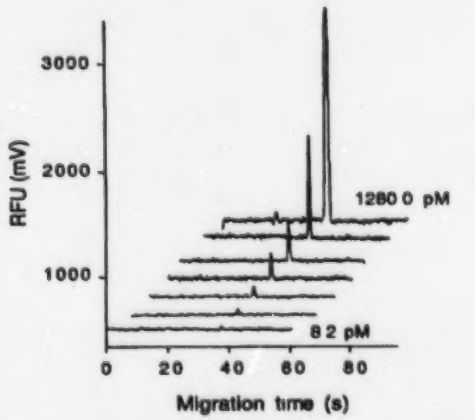

Fig. 7. Electropherograms of various concentrations of Cy-5 standard solutions in a 20 μm deep, DARPA1-NC device. Injection time 10 s at −2 kV injection voltage. Separation voltage was −4 kV. Injector–detector distance was 58 mm, PMT voltage 900 V.

it is larger than the channel depth, and equal to the channel depth when the calculated value is smaller. Although the agreement with theory is only moderate, the sectioning power does lead to observation of a smaller detection zone than the estimated depth of field of the focused laser spot.

Figure 6 shows the trends of S/N versus pinhole size measured by a continuous-flow experiment. The continuous increase in S/N with increasing pinhole size observed for the 13 μm deep channels is not consistent with true confocal performance, while the 20 μm device showed a clear optimum pinhole size of 400 μm. This value is in agreement with our previous study using a 488 nm Ar ion laser, and fluorescein in 30 μm deep channels (Ocvirk et al., 1998). The results can be explained by considering the excitation volume created by the laser beam and the probe volume observed by the confocal microscope. The beam waist can be treated as a constant across the channel depth, so that the excitation volume is a cylinder given by the beam waist. The probe volume can also be treated as a cylinder with a height given by the observed sectioning power or channel depth, and a diameter given by the pinhole size divided by the magnification (40×). For the unexpanded beam the 800 μm pinhole gives a probe diameter which most closely matches the excitation volume, optimizing the collection of all intensity generated by the laser. For the expanded beam, the 400 μm pinhole should best match the estimated probe volume of 1.6 pl to the 10 μm diameter excitation volume of 1.6 pl. Since none of the pinholes gave sufficient sectioning power to eliminate scatter from the glass walls, the best match of probe diameter and beam diameter would give the best results, consistent with observations.

3.4. Limit of detection with optimized parameters

Once an optimal set of detection parameters was determined, the best detection limits were evaluated for an injected and separated sample plug. Figure 7 shows a series of injected sample plugs for a 20 μm deep DARPA1-NC device. A similar data set was obtained with a 13 μm deep DARPA1-NC device. The studies were performed with an expanded beam at 11.2 mW output power, using the optimized filter set and a 400 μm pinhole. For the 13 μm deep device, the detection limit extrapolated from concentrations above 32.8 pM to a S/N of 3, was 20 pM. A calibration curve forced through the origin gave a slope of 0.159 ± 0.013 and an $R^2 = 0.9994$ ($n = 18$). The lowest concentration we were actually able to determine was 32.8 pM. For a 20 μm deep device the extrapolated LOD was 9 pM, and the lowest concentration we were able to determine was 8.2 pM. A calibration curve forced through the origin gave a slope of 0.335 ± 0.012, with $R^2 = 0.9986$ ($n = 21$). This concentration detection limit is somewhat better than the 50–100 pM results obtained with a red diode laser reported for Cy-5 in a conventional fused silica capillary (Chen et al., 1993; Chen, 1995; Mank and Yeung, 1995). It is also better than the present commercial 635 nm LIF system, which, in our hands, gives a 100 pM detection limit with a 50 μm diameter capillary and a 3–5 mm long sample plug.

About 42 000 theoretical plates were achieved with these devices. For an injector to detector length of 5.8 cm, this plate number corresponds to a peak variance (σ^2) of 8.0×10^{-4} cm^2. If we assign all dispersion either to diffusion, or to the sample plug length, we can obtain an upper limit of the plug length using Eq. (4) (Seiler et al., 1993):

$$l^2/12 = \sigma^2 - 2Dt \quad (4)$$

P514973.PDF [Page: 10 of 12]

where l is the estimated injected length, D is the diffusion coefficient (approximated as 3.3×10^{-6} cm^2/s), (Seiler et al., 1993; Fan and Harrison, 1994) and t is the migration time. Eq. (4) provides an estimate of 834 μm for the injected plug, suggesting some leakage at the injector. At the extrapolated LOD the amount of sample volume estimated from this length corresponds to 5900 molecules for the 13 μm deep device at 20 pM, and 4560 molecules for the 20 μm deep device at 9 pM. The number of molecules that entered the detection zone was 1300 and 900, for the 13 and the 20 μm deep devices, respectively, given that the probing efficiencies were 22 and 20% for the 13 and 20 μm deep devices, respectively (probing efficiency is taken as the ratio of the sample volume measured to the total sample volume injected). This mass detection limit is much better than that we achieved with the commercial 635 nm LIF system. It is comparable to the best results reported in conventional CE, which are ~300 molecules when using a red diode laser (Mank and Yeung, 1995).

The observed concentration LOD is about a factor of ten poorer than we reported for fluorescein in a 30 μm deep device (Ocvirk et al., 1998). A further improvement might be observed if we used 30 μm deep channels with the diode laser, since the sectioning power of a 400 μm pinhole is high enough to eliminate scattering from the walls of a 30 μm deep device. The sectioning power study shows that the correction optics supplied with this laser do not generate a truly Gaussian beam, which limits the ability to focus a tight, high intensity spot. More complex optics could be used to improve the beam, but this would be at the expense of laser power and require components that make the detector less easy to place in the field. The background output of the laser required a notch transmittance filter be used, as is often done with gas lasers. It is possible another manufacturer's laser could produce better results in terms of increased focus or lower background emissions. Consequently, detection limits on a chip of 10^{-12} M or less, as obtained with the 488 nm laser/fluorescein system, may yet be achievable with Cy-5 and a diode laser.

4. Conclusions

Red, solid state diode lasers provide a convenient, compact and rugged source for instruments that are to be used in the field. This study illustrates that the 635 nm laser is compatible with detection of immunological reaction products on a planar microfluidic device. It is clear that the performance of the diode laser played a role in the final detection limit, due to issues related to the beam shape and background emissions. Further improvements in diode laser technology should result in better detection limits in the future. Nevertheless, optimization of the optics for detection with this laser allows the determination of a few thousand Cy-5 molecules per sample plug in a electrophoretic separation, with a concentration detection limit of approximately 9 pM in a 20 μm deep channel. This result is five to ten times better than previously reported for red diode lasers in conventional CE, indicating that high performance detection on a chip is achievable with these lasers.

Acknowledgements

We thank the Defense Advanced Research Projects Agency, and Defence Research Establishment Suffield for financial support of this project; Y. Ning of Alberta Microelectronic Corporation for device fabrication, and N. Chiem for the device layouts. We are grateful to M. Paulson of Dycor Industrial Research for identifying laser and filter suppliers.

References

Chen, F T A, 1995 Characterization of protease-catalyzed hydrolysis of cyanine-labeled angiotensin using capillary electrophoresis with laser-induced fluorescence detection Anal Biochem 225, 341–345

Chen, F.T A, Tusak, A, Pentoney, S Jr, Konrad, K, Lew, C, Koh, E, Sternberg, J, 1993 Semiconductor laser-induced fluorescence detection in capillary electrophoresis using a cyanine dye J Chromatogr A 652, 355–360

Chiem, N H, Harrison, D J, 1998a. Microchip systems for immunoassay an integrated immunoreactor with electrophoretic separation for serum theophylline determination Clin. Chem. 44, 591–598.

Chiem, N.H, Harrison, D J., 1998b. Monoclonal antibody binding affinity determined by microchip-based capillary electrophoresis Electrophoresis 19, 3040–3044

Chiem, N H, Harrison, D J, 1997 Microchip-based capillary electrophoresis for immunoassays analysis of monoclonal antibodies and theophylline Anal Chem 69, 373–378

Chu, Y H, Lees, W J, Stassinopoulos, A, Walsh, C, 1994 Using affinity capillary electrophoresis to determine binding stoichiometrics of protein–ligand interactions Biochemistry 33, 10616–10621

Colyer, C L, Tang, T, Chiem, N, Harrison, D J, 1997 Clinical potential of microchip capillary electrophoresis systems Electrophoresis 18, 1733–1741

Effenhauser, C S, Bruin, G J M, Paulus, A, 1997. Integrated chip-based capillary electrophoresis Electrophoresis 18, 2203–2213

Fan, Z H, Harrison, D J, 1994 Micromachining of capillary electrophoresis injectors and separators on glass chips and evaluation of flow at capillary intersections Anal Chem 66, 177–184

Flanagan, J H, Legendre, B L, Hammer, R P, Soper, S A, 1995 Binary solvent effects in capillary zone electrophoresis with ultrasensitive near-IR fluorescence detection of related tricarbocyanine dyes and dye-labeled amino acids Anal Chem 67, 341–347

Grossman, P D, Colburn, J C., Laurer, H H, Neilsen, R G, Riggin, R M, Sittampalam, G S, Rickard, E C, 1989. Application of free-solution capillary electrophoresis to the analytical scale separation of proteins and peptides Anal Chem 61, 1186–1194

P514973.PDF [Page: 11 of 12]

Hadd, A.G., Raymond, D.E., Halliwell, J.W., Jacobson, S., Ramsey, J.M., 1997. Microchip device for performing enzyme assays. Anal. Chem. 69, 3407.

Harrison, D.J., Fluri, K., Seiler, K., Fan, Z., Effenhauser, C.S., Manz, A., 1993. Micromachining a miniaturized capillary electrophoresis-based chemical analysis system on a chip. Science 261, 895–897.

Hecht, E., Zajac, A., 1974. Optics. Addison-Wesley, Reading, MA.

Imasaka, T., 1996. Laser spectroscopy on organic molecules. Fresenius J. Anal. Chem. 355, 216–221.

Imasaka, T., Nishitani, K., Ishibashi, N., 1991. Cyclodextrin-modified micellar electrokinetic chromatography combined with semiconductor laser fluorimetry. Analyst 116, 1407–1409.

Jacobson, S.C., Hergenroder, R., Koutney, L.B., Warmack, R.J., Ramsey, J.M., 1994. Effects of injection schemes and column geometry on the performance of microchip electrophoresis devices. Anal. Chem. 66, 1107–1113.

Jansson, M., Roeraade, J., 1993. Laser-induced fluorescence detection in capillary electrophoresis with blue light from a frequency-doubled diode laser. Anal. Chem. 65, 2766–2769.

Krattiger, B., Bruin, G.J.M., Bruno, A.E., 1994. Hologram-based refractive index detector for capillary electrophoresis: separation of metal ions. Anal. Chem. 66, 1–8.

Mank, A.J.G., Yeung, E.S., 1995. Diode laser-induced fluorescence detection in capillary electrophoresis after pre-column derivatization of amino acids and small peptides. J. Chromatogr. A 708, 309–321.

Manz, A., Harrison, D.J., Verpoorte, E.M.J., Fettinger, J.C., Paulus, A., Lüdi, H., Widmer, H.M., 1992. Planar chips technology for miniaturization and integration of separation techniques into monitoring systems. J. Chromatogr. 593, 253–258.

McDonnell, T., Pawliszyn, J., 1991. Capillary isotachophoresis with concentration gradient detection. Anal. Chem. 63, 1884–1889.

Narang, U., Gauger, P.R., Ligler, F.S., 1997. A displacement flow immunosensor for explosive detection using microcapillaries. Anal. Chem. 69, 2779–2785.

Ocvirk, G., Tang, T., Harrison, D.J., 1998. Optimization of confocal epifluorescence microscopy for microchip-based miniaturized total analysis systems. Analyst 123, 1429–1434.

Schmalzing, D., Nashabeh, W., 1997. Capillary electrophoresis based immunoassays. a critical review. Electrophoresis 18, 2184–2193.

Shriver-Lake, L.C., Breslin, K.A., Charles, P.T., Conrad, D.W., Golden, J.P., Ligler, F.S., 1995. Detection of TNT in water using an evanescent wave fiber-optic biosensor. Anal. Chem. 67, 2431–2435.

Seiler, K., Harrison, D.J., Manz, A., 1993. Planar glass chips for capillary electrophoresis: repetitive sample injection, quantitation, and separation efficiency. Anal. Chem. 65, 1481–1488.

Tao, L., Kennedy, R.T., 1996. On-line competitive immunoassay for insulin based on capillary electrophoresis with laser-induced fluorescence detection. Anal. Chem. 69, 3899–3906.

Wilson, T.J., 1989. Optical sectioning in confocal fluorescent microscopes. J. Microsc. 154, 143–156.

Wilson, T., 1990. In: Pawley, J.B. (Ed.), Handbook of Biological Confocal Microscopy. Plenum, New York, pp. 113–126.

Wu, J., Frank, P., Pawliszyn, J., 1992. Diode laser-based concentration gradient detector for detection of capillary isoelectric focusing. Appl. Spec. 46, 1837–1840.